04

Investigation of emission properties of nitrogen capillary plasma in the water windowregion: interpretation of experimental data based on magnetohydrodynamic modeling

© A.A. Samokhvalov,[1,2] K.A. Sergushichev,[2] S.I. Eliseev,[2,3] T.P. Bronzov,[2] E.P. Bolshakov,[2] D.V. Getman,[2] A.A. Smirnov[2]

[1] ITMO University,
197101 St. Petersburg, Russia
[2] Laboratory them. V.A. Burtseva,
197022 St. Petersburg, Russia
[3] St. Petersburg State University,
199034 St. Petersburg, Russia
e-mail: andreia.sam@yandex.ru, samokhvalov.itmo@gmail.com

Received April 14, 2024
Revised April 14, 2024
Accepted April 14, 2024

This paper presents experimental and numerical results on radiation generation in the „water window“region. Based on the MHD model, the interpretation of the experimental results obtained on a compact gas-discharge radiation source was carried out. The data obtained makes it possible to carry out multiparametric optimization of gas-discharge radiation sources.

Keywords: capillary discharge, highly charged ions, emission spectroscopy, magnetohydrodynamics, numerical modeling.

DOI: 10.61011/TP.2024.07.58795.123-24

Introduction

Transmission microscopy the „water window“ spectral band, i.e. in the 2.3−4.4 nm band is used for contrast microscopy and tomography of cell cultures and biological objects, detect various viruses and cell abnormalities with high resolution. Recently it has been shown [1] that, when using diffraction optics — zone plates — the resolution of this method may achieve ~ 10 nm. Synchrotrons have been traditionally used as a „water window“ radiation source, but it is obvious that research facilities on such scale are available to only very few research teams.

Therefore, alternative desktop radiation sources have been created at this point. Laser plasma is one of the effective sources. This type of sources uses a gas target formed using a special nozzle [2]. The key advantages of this type of sources include high spectral radiance, no impurity bands and no target disintegration products in a vacuum system. Laser plasma radiation is known to be omnidirectional and requires special multilayer mirrors for transportation, their efficiency in the given 2.3−4.4 nm band achieves $\sim 5\%$ [3]. With relatively low conversion of laser energy into plasma radiation, efficiency of such types of sources may be improved due to using high pulse repetition rate (more than 1 kHz) lasers at high energy in the pulse itself; the typically required pulse energy is more than 100 mJ.

Gas-discharge plasma generated in gas breakdown is another „water window“ radiation source. For this type of radiation sources, high-voltage generator and discharge geometry are essential and generally define the gas-discharge source efficiency. In these sources, the radiation spectrum is often contaminated with spectral lines of the material elements from which the capillary is made, therefore a problem of capillary wall ablation reduction often occurs in the capillary plasma formation process. On the other hand, the capillary plasma has a feature — low divergence due to the Z-pinch radiation self-focusing effect at high currents. Two approaches to design of such sources are distinguished. In the first case (pseudo spark sources), electric energy is accumulated due to high capacity of the capacitor unit (units of μF) and the voltage level does not exceed 10 kV [4]. In the other case (capillary plasma sources) [5], the capacity is not higher than units of nF and energy is accumulated due to high-voltage pulses with amplitude $\sim 20-30$ kV. Note that for both approaches, sources generating „water window“ radiation with frequencies more than 1 kHz were successfully created. However, the discharge module life is one of the critical aspects of real applications of these sources. In the first case, the discharge cavity was made from molybdenum alloy and had complex configuration, in the second case — plasma was initiated in a thin ceramic capillary. Replacement of the ceramic capillary is apparently a more affordable operation.

A plasma property control function is another advantage of capillaries made of various materials with various geometrical parameters. Thus, the authors of [6] have shown that the line of helium-like ion N VI on 2.88 nm is observed in the capillary plasma radiation spectrum even at low

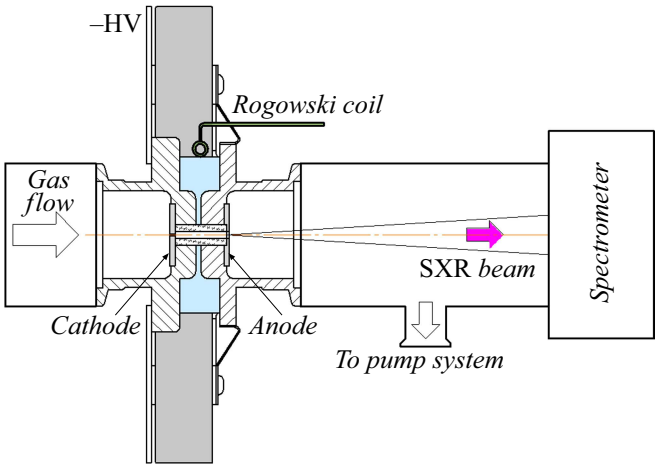

Figure 1. Experimental setup with main assemblies.

energy level input in the plasma when a capillary with a corresponding diameter is chosen. For comparison, the pseudo spark source energy for achievement of spectral line N VI — 2.88 nm — was equal to 14 J [7], and maximum 1 J in the capillary radiation source. In this case, the energies in the obtained optical pulses were comparable. Plasma geometry depends both on the discharge geometry and on the energy input method, therefore the pseudo spark source does not provides flexibility in plasma parameter variation. This feature was faced by the authors of [7] when matching the radiative plasma geometry with the optical microscopy system.

Thus, for successful employment of gas-discharge sources, it is necessary to use a comprehensive approach that shall be based on experimental research methods and on numerical simulation that allows interpreting and predicting the behavioral features and physical parameters of the gas-discharge plasma.

The study investigates the capillary plasma spectra in the „water window“ range to improve the performance of the compact radiation source which was used for the experiments. For experimental findings analysis, a magnetohydrodynamic (MHD) model was developed to assess electrophysical and geometrical parameters of the capillary plasma.

1. Experimental setup

The design of a compact capillary-discharge soft X-ray radiation (SXR) source and the measurement equipment were detailed in our previous study [8]. However, the paper describes some features of the experiments.

The capillary was made of VK-95 (Al_2O_3) ceramics, capillary ID was 1.6 mm, length was 20 mm. Although, in our previous study [8], we have shown that a silicon nitride capillary has the best performance, we have intentionally took this material for greater clarity in the experiments and to compare our emission spectroscopy data with the literature data.

Capillary plasma emission spectra were recorded using the GIS-2 grazing incidence spectrometer with a 1200 groove diffraction grating, and the GreatEyes GE 1024 1024 BI UV1 CCD camera was used as a detector, spectrometer's spectral resolution $\lambda/\Delta\lambda$ was ~ 200.

Current pulses were measured by the Rogowski coil, and a high-voltage divider was used to measure voltage pulses. All signals were recorded using the Tektronix DPO-DPO7104C four-channel oscilloscope in a bandwidth of 1 GHz and averaged over 20 pulses; the spectra were also averaged over 20 discharges.

Our source features a fast effective capacity change function consisting of ceramic capacitors placed coaxially to the capillary. We could vary the amount of accumulated electric energy by measuring the number of capacitors and capacity of a single capacitor, and the charge voltage varied from 15 to 25 kV for the purpose of our experiments. Based on design aspects of the setup and technological features of the high-voltage generator, three capacities were used: 5.4, 8 and 10.8 nF. Thus, with various capacity and voltage combinations, the energy stored in the capacitors was from 1 to 3.5 J. The experiments used extra pure grade nitrogen (99.99%) was used as working gas, the capillary inlet pressure for the experiments was equal to 1.5 Torr.

2. Findings and discussion

2.1. Experimental findings

Spectral radiance of plasma is defined by the density of plasma particles, however, it is necessary to distinguish at least two limiting cases — when plasma is optically thin at optical density $\tau \ll 1$ and optically dense at $\tau \gg 1$ [9]. In the first case, spectral radiance L in the lines depends linearly on the particle concentration and is defined by expression (1), in the second case, we have in the limit the Planck spectrum and line radiation self-absorption in the continuum (2):

$$L \sim e^{(-\Delta E/T_e)} T_e^{-1/2} n_e n_i f d, \tag{1}$$

$$L \sim \frac{1}{\lambda^4} \frac{1}{e^{(\Delta E/T_e)} - 1} \left(\frac{\Delta\lambda}{\lambda}\right) R(\tau), \tag{2}$$

where $\Delta E, \lambda$ is the energy and corresponding transition wavelength, T_e is the electron temperature, n_e, n_i are electron and ion densities, respectively, f is the oscillator force, d is the plasma column length, $R(\tau)$ is the self-absorption coefficient.

The latter limits the plasma efficiency as the radiation source. In particular, for the „water window“ microscopy purposes, this may reduce the contrast and resolution. Thus, when a continuous spectrum occurs near the spectral line, it almost cannot be isolated because the existing filters and mirrors have a wide spectral range in comparison with a single spectral line.

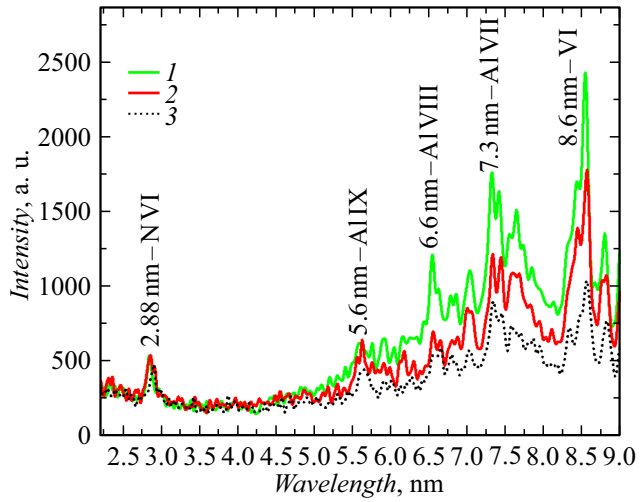

Figure 2. The capillary discharge emission spectra in nitrogen at an input energy of 1.7 J for different capacity options: *1* — 5.4 nF (25 kV), *2* — 8 nF (20 kV), *3* — 10.8 nF (18 kV).

On the other hand, real facilities always have technical limits associated with high-voltage generators, discharge geometry, system inductance and other engineering features. Gas-discharge radiation sources can accumulate energy in two ways, the first case — by high-capacity charging with relatively low voltages, the second inverse case — by low-capacity charging with higher amplitude voltage. Since the accumulated energy is quadratically dependent on voltage $E = (CU^2)/2$, and the charging time of the capacitor bank grows with its capacity, the second option is more preferable. On the other hand, as the charging voltage increases, requirements for dielectric strength and shielding of the whole structure grow, and induced interference level in the instrumentation increases. Therefore, in real conditions, it is necessary to perform multiparameter optimization of a gas-discharge radiation source as applicable using quantitative and qualitative comparison of the spectral parameters of gas-discharge plasma radiation.

Our experimental setup allowed the energy accumulated in the capacitor bank to be varied by changing the number of capacitors and charging voltage amplitude. Capillary plasma radiation spectra were recorded experimentally at various energy levels accumulated in the capacitor bank. The setup had three discrete capacities — 5.4, 8 and 10.8 nF; by varying the charging voltage, we could achieve the equivalent energy accumulation with various number of capacitors. Figure 2 shows the capillary discharge spectra measured at ~ 1.7 J for the capacities listed above.

As shown in Figure 2, with the equivalent stored energy (~ 1.7 J), the spectra differ significantly for different capacities. The intensity of helium-like nitrogen ion N VI on 2.88 nm in case of the maximum possible capacity (10.8 nF) is a little lower than that in two other cases with capacities of 5.4 and 8 nF. On the other hand, for the minimum capacity of 5.4 nF, we observe significant increase in radiance intensity of line Al IX, which indicates considerable capillary wall ablation. In the latter case, the charging voltage was 25 kV, in two other cases — 20 kV at 8 nF and 18 kV at 10.8 nF. Note that for these experiments, we used the maximum charging voltage of 25 kV to ensure the dielectric strength of the capillary unit and the absence of interference induced in the instruments.

Thus, with the equivalent energy stored in the capacitor bank, it is more preferable to increase the capacity with simultaneous charging voltage reduction in terms of wall ablation reduction and capillary life extension. Then, dependences of the radiance intensity of ion N VI and Al IX lines on the stored electric energy were obtained throughout the available experimental operating voltage range, see Figure 3, 4.

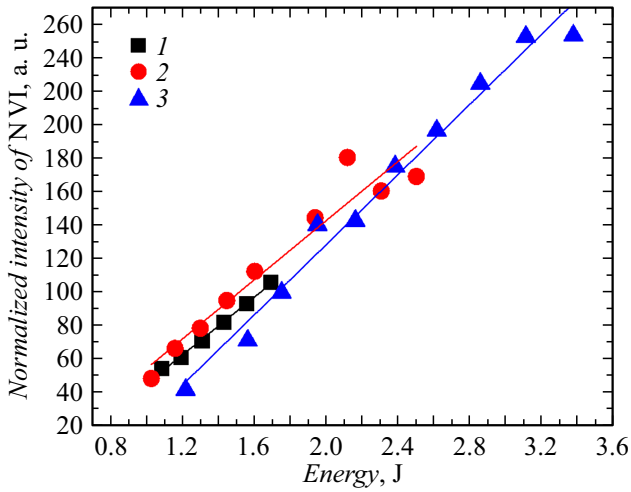

Figure 3. Dependence of radiance intensity of N VI line on the energy input to the capillary plasma at different capacities: *1* — 5.4, *2* — 8, *3* — 10.8 nF.

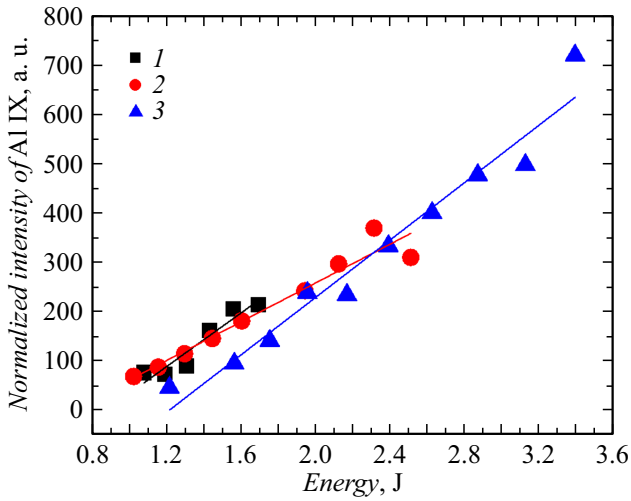

Figure 4. Dependence of radiance intensity of Al IX line on the energy input to the capillary plasma at different capacities: *1* — 5.4, *2* — 8, *3* — 10.8 nF.

As shown in Figure 3, the N and Al line intensities depend linearly on the energy input to the plasma for all three capacity combinations. However, for 8 and 10.8 nF, with experimentally achievable peaks, saturation of these dependences is observed. For energies up to 2.2 J, the nitrogen line N VI has the highest intensity at 8 nF, with further increase in the input energy, the capillary wall ablation intensity grows considerably, which is shown by the increase in the intensity of line Al IX compared with that of line N VI.

It follows from the dependences shown in Figure 3, 4 that the capillary ablation may be reduced by using a higher capacity at lower voltages with simultaneous increase in the radiation intensity of helium-like nitrogen line N VI. However, the qualitative analysis makes it possible to seen some singularities on the emission spectra due to which the maximum capacity option is inappropriate: Figure 5 shows the spectra at maximum voltage for 8 and 10.8 nF.

As shown in Figure 5, multicharged ions N VII and Al XI occur in the spectrum, and at the same time the capillary wall ablation intensity grows considerably: Al line intensity is much higher than the N line intensity. It is expected that the wall ablation process affects the degree of gas ionization. It is interesting that a continuum occurs in the spectrum at the maximum electric pulse energy, with the spectral line located against the background of this continuum. The continuum radiation intensity is known to be defined by photorecombination and inhibitory processes in plasma, which may be studied by the time-resolved spectroscopy. But in terms of microscopy, the continuum will degrade the contrast and resolution of the method. On the other hand, contribution to the observed continuum could be made by the scattered visible light rereflected in the vacuum chamber. To prevent this effect, future experiments with thin-film filters are planned in order to cut out the desired spectrum range.

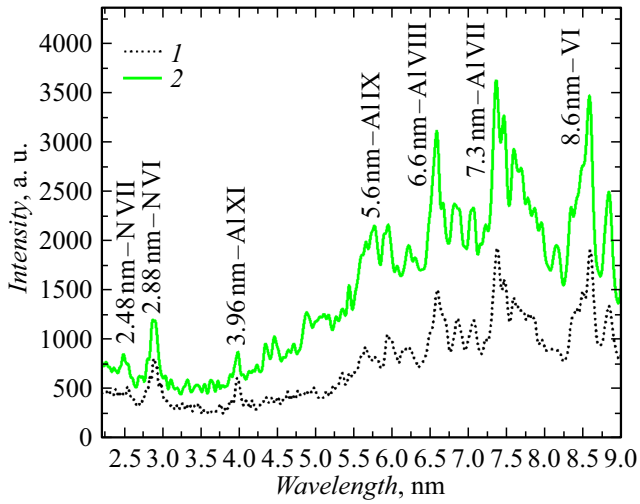

Figure 5. Nitrogen capillary plasma spectra for different capacities: *1* — 8, *2* — 10.8 nF, charging voltage in both cases is 25 kV.

Thus, the experiments show that a capacity of 8 nF is the best for out setup because it provides high intensity of N line on 2.88 nm and minimizes the capillary wall ablation intensity. However, for detailed analysis of physical processes and to choose the best radiation generation conditions in the „water window“ region, they shall be addressed in detail using numerical simulation.

2.2. Numerical simulation results

Plasma behavior in the given nanosecond capillary conditions was reproduced by numerical solution of the system of MHD equations written to the two-temperature one-fluid approximation. The approach is based on the assumption that the local thermodynamic equilibrium is met separately for the electronic and ionic components. Considering the low longitudinal inhomogeneity and azimuthal symmetry of the plasma column throughout the discharge, the key quantities of interest — magnetic field strength H, plasma density ρ, radial plasma velocity v, electron and ion temperatures T_e, T_i — may be obtained as functions of only one spatial coordinate — capillary radius r.

In case of capillary discharges, the system of MHD equations is usually written in the Lagrangian coordinates making it possible to define the problem compactly and to better describe the plasma separation from the capillary wall. In the Lagrangian statement, observation follows some plasma „element“ (or „particle“), rather than is fixed in the given point in space. Thus, plasmodynamic quantities defined as functions of the Lagrangian coordinates describe the properties of each plasma „element“ in time. Any quantity that formally allows distinguishing these elements may be a Lagrangian coordinate [10,11]. Though there are multiple ways to determine the Lagrangian spatial coordinates, our model used the initial radial position of a plasma element r_0 [10,11]. In this case, spatial derivatives in the MHD equations may be written as [13]:

$$\frac{\partial}{\partial r} = \frac{\rho\tilde{r}}{\rho_0 r_0}\frac{\partial}{\partial r_0}.$$

Here, $\rho = \rho(r_0, t)$ is the spatial distribution of plasma density over the capillary radius, $\tilde{r} = \tilde{r}(r_0, t)$ is the Euler spatial coordinate of this plasma element, $\rho_0 = \rho_0(r_0)$ is the initial spatial distribution of plasma density. Together with time derivatives ratio in different frames of reference:

$$\frac{\partial}{\partial t} = \frac{\partial}{\partial t} + v\frac{\partial}{\partial r} = \frac{\partial}{\partial t_L},$$

where d/dt is the total derivative with respect to time, $\partial/\partial t_L$ is the derivative with respect to time in the Lagrangian coordinate system, v is the plasma velocity, the system of MHD equations can be rewritten as (in SI units):

$$\frac{d\rho}{dt_L} + \frac{\rho^2}{\rho_0 r_0}\frac{\partial \tilde{r} v}{\partial r_0} = 0,$$

$$\rho\frac{\partial v}{\partial t_L} + \frac{\rho\tilde{r}}{\rho_0 r_0}\frac{\partial}{\partial r_0}(p + \Pi_{rr}) = -\mu_0 j_z H - \frac{1}{\tilde{r}}(\Pi_{rr} - \Pi_{\varphi\varphi}),$$

$$\rho_0 r_0 \frac{\partial \varepsilon_e}{\partial t_L} + \frac{\partial}{\partial r_0}(\tilde{r} W_e) = (j_z E_z - Q_R - Q_{ei}) \times \frac{\rho_0 r_0}{\rho} - p_e \frac{\partial v \tilde{r}}{\partial r_0},$$

$$\rho_0 r_0 \frac{\partial \varepsilon_i}{\partial t_L} + \frac{\partial}{\partial r_0}(\tilde{r} W_i) = \left(\frac{v}{\tilde{r}}(\Pi_{rr} - \Pi_{\varphi\varphi}) + Q_{ei}\right) \frac{\rho_0 r_0}{\rho} - (p_i + \Pi_{rr}) \frac{\partial v \tilde{r}}{\partial r_0},$$

$$\frac{\partial}{\partial t} \frac{H_\varphi}{\rho} - \frac{\tilde{r}}{r_0 \rho_0} \frac{\partial}{\partial r_0} \frac{E_z}{\mu_0} = \frac{H_\varphi v}{\rho \tilde{r}},$$

$$\frac{d\tilde{r}}{dt} = v.$$

Here, ε_e and ε_i are the electron and ion energy densities in J/kg; H_φ is the azimuthal component of the magnetic field strength vector; $p = p_e + p_i$ is the plasma pressure defined as the sum of electron and ion pressures; $Q_{ei} = C_{ei} k_B (T_e - T_i)$ is the heat exchange rate between the electronic and ionic components of plasma (k_B is the Boltzmann constant); Q_R is radiation-induced energy loss; μ_0 is the magnetic permeability of vacuum. The longitudinal current density component j_z and electric field E_z were calculated (including the Nernst effect) as

$$j_z = \frac{\rho}{\rho_0 r_0} \frac{\partial}{\partial r_0}(\tilde{r} H_\varphi),$$

$$E_z = \frac{j_z}{\sigma} - N \mu_0 H_\varphi k_B \frac{\rho r}{\rho_0 r_0} \frac{\partial T_e}{\partial r_0},$$

Π_{rr} and $\Pi_{\varphi\varphi}$ are radial and azimuthal components of the viscosity tensor (only ionic viscosity was considered, electronic viscosity was neglected):

$$\Pi_{rr} = \frac{2}{3} \eta_0 \left(\frac{v}{\tilde{r}} - 2 \frac{\rho \tilde{r}}{\rho_0 r_0} \frac{\partial v}{\partial r_0}\right),$$

$$\Pi_{\varphi\varphi} = \frac{2}{3} \eta_0 \tilde{r}^3 \frac{\rho}{\rho_0 r_0} \frac{\partial}{\partial r_0}\left(\frac{v}{\tilde{r}^2}\right),$$

W_e and W_i are thermal electron and ion fluxes calculated (including the Ettingshausen effect) as

$$W_{e,i} = -\varkappa^e_\perp k_B \frac{\rho \tilde{r}}{\rho_0 r_0} \frac{\partial T_e}{\partial r_0} + N \mu_0 H_\varphi k_B T_e j_z,$$

$$W_i = -\varkappa^i_\perp k_B \frac{\rho \tilde{r}}{\rho_0 r_0} \frac{\partial T_i}{\partial r_0}.$$

For the ionic component, the ideal gas approximation was used

$$\varepsilon_i = \frac{3}{2} \frac{k_B}{M_i} T_i, \quad p_i = \frac{\rho}{M_i} k_B T_i.$$

It was assumed that the electronic component consists of free and bound electrons. Free electron gas is the ideal gas, and the ionization energy was introduced into the expression for electron energy density:

$$\varepsilon_e = M_i^{-1}\left(\frac{3}{2} k_B T_e + U(\bar{Z})\right), \quad p_e = \bar{Z} \frac{\rho}{M_i} k_B T_e,$$

where $U(\bar{Z})$ is the ionization potential, $\bar{Z}$ is the mean ion charge calculated using the Raizer approach approximation and averaged ion model [12]. Both the electron temperature and average ion charge were summarized in tables as function of electron energy densities and plasma densities and used as external parameters of the numeric model. The calculation procedure is described in detail in [13,14]. Plasma conductance σ, ionic viscosity η_0, electronic and ionic thermal conductivities $\varkappa_{e,i}$, heat transfer rate C_{ei} and Nernst coefficient N were defined as described in [14]. To estimate typical plasma channel compression times, plasma channel radius variation was calculated as shown in Figure 6, the working gas pressure of 1.5 Torr was taken from the experimental conditions. The typical temporal behavior of plasma parameters at a breakdown voltage of 15 kV is shown in Figure 7.

Figure 6 shows that as the breakdown voltage increases, the maximum compression time and the plasma channel diameter decrease. And as shown in Figure 7, the maximum compression is achieved near the time of achievement of the current peak suggesting that effective energy contribution to plasma is implemented in the experimental conditions.

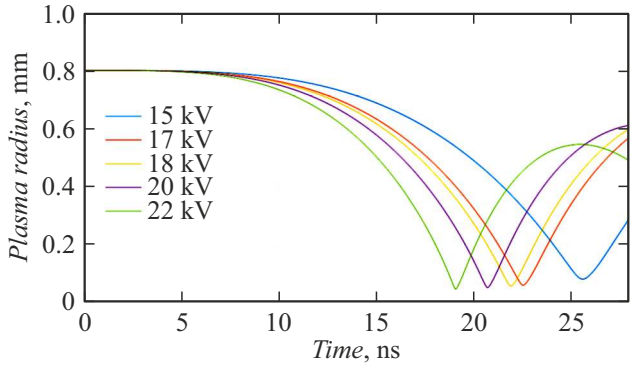

Figure 6. Temporal behavior of the plasma channel radius with different discharge currents (voltages).

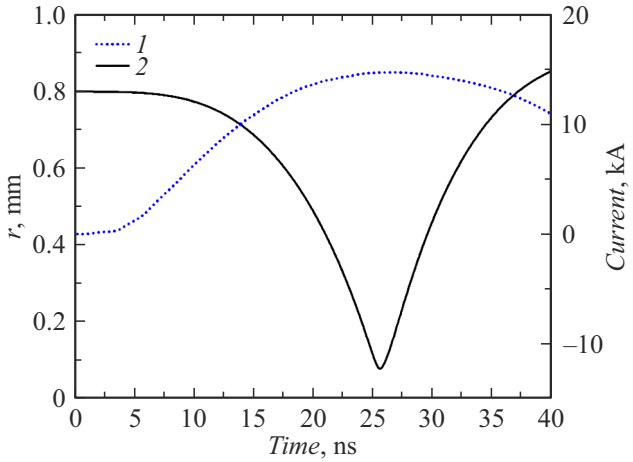

Figure 7. Typical temporal behavior of plasma parameters at a breakdown voltage of 15 kV: *1* —experimentally obtained current pulse, *2* — simulated plasma radius.

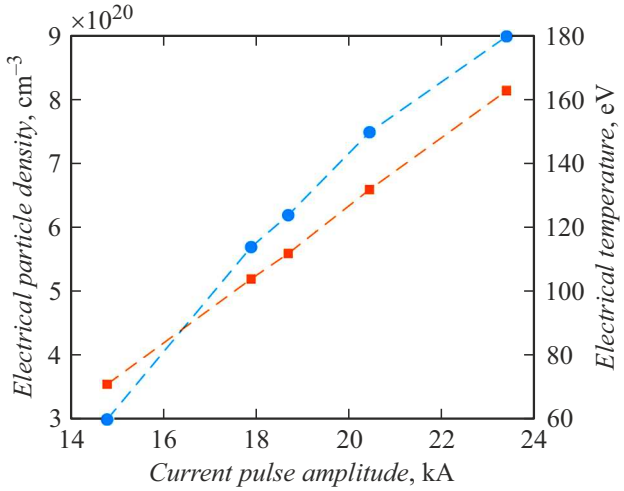

Figure 8. Dependence of the electron density and temperature on the maximum current amplitude in the nitrogen capillary plasma.

Figure 8 shows dependences of electron concentration and temperature on discharge current amplitude.

As shown in Figure 8, both the electron concentration n_e and electron temperature T_e correlate linearly with the current amplitude, however, note that 50% increase in current results in the multiple growth of maximum values of n_e (by a factor of 3) and T_e (by a factor of 2). On the other hand, as can be seen on the emission spectra (Figure 2, 5), the capillary wall ablation intensity grows together with the degree of plasma ionization. This suggests that the wall ablation process influences the ionization composition of plasma and generally increases its degree of ionization. However, by increasing the gas pressure and/or capillary diameter for molecular gases, the capillary wall ablation intensity may be reduced considerably.

The MHD simulation results, in turn, are used to define the transverse dimension of plasma; the appropriate measurements were performed in [15] using argon. This parameter is essential for design and construction of optical systems for „water window“ microscopy.

According to the simulation results, we can see how the current amplitude may be used to forecast the transverse diameter of plasma and how this value defines the key plasma parameters that depend linearly on the current amplitude. On the other hand, the experimental data are used to observe the linear dependence of the radiance intensity of multicharged ion lines on the energy input into plasma. Thus, we can claim that the calculation results agree well with the experimental data and may be used for future improvement of gas-discharge radiation sources of this type.

Conclusion

The paper describes the experimental findings obtained for the gas-discharge soft X-ray source and numerical simulation of physical processes in the nitrogen capillary plasma. It is shown that energy input into plasma due to electric energy accumulation in the capacitor bank is most preferable because it allows the capillary wall ablation intensity to be reduced. Whereas, high voltages used with the equivalent input energy facilitate the ablation process. Linear dependence of the radiance intensity of helium-like ion N NI on the electric energy input into plasma is also shown.

The MHD simulation gave the radiative plasma dimensions and estimated dependence of the key plasma parameters on experimentally measured peak currents. Linear dependence of the electronic density and temperature on the discharge current amplitude was also obtained. The main behavioral patterns of plasma parameters in various experimental conditions were explained.

The MHD model and approach described herein may be used for future improvement of gas-discharge radiation sources and to achieve quasi-monochromatic radiation in the „water window“ region for microscopy of cell cultures and other bio- and nanoobjects.

Funding

The study was performed at „Laboratory named after V.A. Burtsev“ under the grant provided by the Russian Science Foundation (project № 21-79-10110).

Conflict of interest

The authors declare that they have no conflict of interest.

References

[1] M. Kördel. The Optical Society, **7** (6), 658 (2020). DOI: 10.1364/OPTICA.393014
[2] V.E. Guseva, A.N. Nechay, A.A. Perekalov, N.N. Salashchenko, N.I. Chkhalo. ZhTF, **92** (8), 1185 (2022). (in Russian). DOI: 10.21883/TP.2022.08.54563.72-22
[3] E. Fogelqvist, M. Kördel, V. Carannante, B. Önfelt, H.M. Hertz. Sci. Rep., **7** (1), 1 (2017). DOI: 10.1038/s41598-017-13538-2
[4] K. Bergmann, F. Küpper, M. Benk. J. Appl. Phys., **103** (12), 123304 (2008). DOI: 10.1063/1.2940786
[5] E.S. Wyndham, M. Favre, M.P. Valdivia, J.C. Valenzuela, H. Chuaqui, H. Bhuyan. Rev. Sci. Instrum., **81** (9), 093502 (2010). DOI: 10.1063/1.3482070
[6] M.P. Valdivia, E.S. Wyndham, M. Favre, J.C. Valenzuela, H. Chuaqui, H. Bhuyan. Plasma Sources Sci. Technol., **21** (2), 025011 (2012). DOI: 10.1088/0963-0252/21/2/025011.
[7] M. Benk, K. Bergmann, D. Schäfer, T. Wilhein. Opt. Lett., **33** (20), 2359 (2008).
[8] A.A. Samokhvalov, K.A. Sergushichev, S.I. Eliseev, A.A. Smirnov, T.P. Bronzov, D.V. Getman, E.P. Bolshakov, M.V. Timshina, V.A. Burtsev. JINST, **17**, P06002 (2022). DOI: 10.1088/1748-0221/17/06/P06002
[9] Th. Krücken, K. Bergmann, L. Juschkin, R. Lebert. J. Phys. D. Appl. Phys., **37** (23), 3213 (2004). DOI: 10.1088/0022-3727/37/23/002

[10] A. Esaulov, P. Sasorov, L. Soto, M. Zambra. Plasma Phys. Control. Fusion, **43**, 571 (2001).
[11] M. Vrbova, P. Vrba, A. Jancarek, M. Nevrkla, N.A. Bobrova, P.V. Sasorov. Phys. Plasmas, **26**, 083108 (2019). DOI: 10.1063/1.5095606
[12] Y.B. Zel'dovich, Y.P. Raizer. *Physics of Shock Waves and High-Temperature Hydrodynamic Phenomena* (Academic Press, NY., 1967)
[13] A.A. Samarsky, P. Popov. *Raznostnye metody resheniaya zadach gazovoy dinamiki*. Ucheb.posobie dlya buzov, 3-e (dop.) izd. (Nauka, M. (1992) (in Russian).
[14] V.B. Eliseev, S.A. Samokhvalov, Y.P. Zhao. J. Phys. D. Appl. Phys., **55**, 075202 (2021). DOI: 10.1088/1361-6463/ac30b7
[15] A.A. Samokhvalov, S.I. Eliseev, A.A. Smirnov, K.A. Sergushichev, M.V. Timshina. High Energy Chem., **57**, 188 (2023). DOI: 10.1134/S0018143923070408

Translated by E.Ilinskaya